

# Proceedings of the 11th International Conference on Structures in Fire



Editors: David Lange, Cristian Maluk, Kang Hai Tan, Dong Zhang, Yao Zhang,  
Julian Mendez Alvarez, Juan Hidalgo, Felix Wiesner, Martyn McIaggan,  
Abdulrahman Zaben, Wenxuan Wu, Hangyu Xu

**UQ Fire**



**THE UNIVERSITY  
OF QUEENSLAND**  
AUSTRALIA

CREATE CHANGE

**NETZSCH**  
Proven Excellence.

**afac** 

**omnii**  
Consulting Fire Engineers

**Proceedings of the 11<sup>th</sup>  
International  
Conference on  
Structures in Fire**

**Hosted by The University of Queensland**

Proceedings of the 11<sup>th</sup> International Conference on Structures in Fire  
(SiF 2020)

Hosted by The University of Queensland

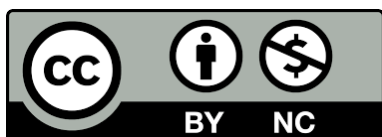
30 November to 2 December 2020

Editors: David Lange, Cristian Maluk, Kang Hai Tan, Dong Zhang, Yao Zhang, Julian Mendez Alvarez,  
Juan Hidalgo, Felix Wiesner, Martyn Mclaggan, Abdulrahman Zaben, Wenxuan Wu, Hangyu Xu

Published by The University of Queensland, Australia © 2020

ISBN: 978-1-74272-343-3

All articles included in this collection are published under a Creative Commons Attribution Non-  
Commercial (CC BY 4.0) License



**Sponsored by:**

**NETZSCH**

Proven Excellence.



**omnii**  
Consulting Fire Engineers

**Organised by:**

**UQ Fire**



CREATE CHANGE



## TABLE OF CONTENTS

Table of contents	v
Preface	xii
Committees	xiv
<b>Applications of structural fire engineering</b>	
A practical tool for evaluating fire induced failure probability of steel columns designed based on U.S. prescriptive standards <i>Ramla Qureshi; Ruben Van Coile; Danny Hopkin; Thomas Gernay; Negar Elhami Khorasani</i>	1
Fire performance of a steel open car park in the light of the recent development of the localised fire model "LOCAFI" <i>Mauro Sommavilla; Nicola Tondini</i>	12
The collapse of World Trade Center 7: revisited <i>Mhd Anwar Orabi; Liming Jiang; Asif Usmani; Jose L. Torero</i>	23
Steel sheet piles exposed to fire experimental tests and numerical modelling <i>Jean-Marc Franssen; João Martins</i>	34
Modelling concrete slabs subjected to localised fire action with OpenSees <i>Liming Jiang; Mhd Anwar Orabi; Jin Qiu; Asif Usmani</i>	46
A framework for reliability-based assessment of structures in post-fire conditions <i>Tom Molkens; Barbara Rossi</i>	55
Influence of time step on stability of the hybrid fire testing in a limited divergence zone <i>Bunthan Iea; Duc Toan Pham; Nicolas Pinoteau; Romain Mege; Jean-François Caron</i>	67
Real-time multi degrees of freedom hybrid fire testing using Pi control <i>Elke Mergny; Jean-Marc Franssen</i>	77
Lifetime economically optimum position of steel reinforcement in a concrete column exposed to natural fire <i>Shuna Ni; Ruben Van Coile; Negar Elhami Khorasani; Danny Hopkin; Thomas Gernay</i>	89

## Composite structures

- Evaluation of the fire performance of unprotected composite beams with fin-plate joints 101  
*N. Yotsumoto; T. Hirahisma; K. Toyoda*
- Effect of steel-fiber reinforced concrete on the fire resistance of concrete-filled steel tubular columns under simultaneous axial loading and double curvature bending 113  
*Takuya Kinoshita; Yusuke Shintani; Tomohito Okazaki; Toshihiko Nishimura; J Y Richard Liew*
- Applicability of the resistance integration method on bonded fasteners loaded in tension in uncracked concrete under ISO 834-1 fire 124  
*Omar Al-Mansouri; Romain Mège; Nicolas Pinoteau; Thierry Guillet; Sébastien Rémond*
- Bond behaviour of elliptical concrete-filled steel tubes after fire exposure 134  
*Tianyi Song; Xialu Liu; Kai Xiang*
- Bonding of grouted eccentric strands in duct at elevated temperatures 146  
*Xiqiang Wu; Francis Tat Kwong Au; Xinyan Huang*
- Experimental study on fire resistance of a full-scale composite floor assembly in a two-story steel framed building 158  
*Lisa Choe; Selvarajah Ramesh; Xu Dai; Matthew Hoehler; Matthew Bundy*
- The role of end conditions on the behaviour of steel-concrete composite beams in fire 171  
*Priya S. Natesh; Anil Agarwal*

## Concrete structures

- Effect of transverse and longitudinal confinement on the interlayer bond in 3D printed concrete at elevated temperatures: an experimental study 184  
*Antonio Cicione; Khanya Mazolwana; Jacques Kruger; Ricahrd Walls; Zara Sander; Gideon Van Zijl*
- Predicting the fire rating of cantilever slab-wall connection with post installed rebar 196  
*Hitesh Lakhani; Jatin Aggarwal; Jan Hofmann*
- Influence of spalling on the biaxial bending resistance of reinforced concrete columns exposed to fire 204  
*David L. Peña; Carmen Ibáñez; Vicente Albero; Ana Espinós; Antonio Hospitaler; Manuel L. Romero*
- Effect of non-uniform heating and cooling on eccentrically loaded reinforced concrete columns 212  
*Jamie Maclean; Luke Bisby; Carmen Ibáñez*
- Bond behavior between reinforcing steel bars and concrete at elevated temperatures 222  
*Ira Banoth; Anil Agarwal*
- Post-earthquake fire assessment of reinforced concrete columns 230  
*Hemanth Kumar Chinthapalli; Anil Agarwal*

Damage assessment framework for tunnel structures subjected to fire <i>Nan Hua; Anthony Frederick Tessari; Negar Elhami Khorasani</i>	242
Comparative fire behavior of reinforced concrete beams made of different concrete strengths <i>Venkatesh Kodur; Srishti Banerji</i>	254
Modeling the structural behavior of reinforced concrete walls under ISO fire exposure <i>Mohsen Roosefid; Marie Helene Bonhomme; Pierre Pimienta</i>	262
Numerical investigation of the structural response of eccentrically loaded reinforced concrete columns exposed to non-uniform heating and cooling <i>Patrick Bamonte; Nataša Kalaba; Jamie Maclean; Luke Bisby</i>	271
Global resistance factor for the burnout resistance of concrete slabs exposed to parametric fires <i>Thomas Thienpont; Ruben Van Coile; Balsa Jovanovic; Wouter De Corte; Robby Caspeele</i>	282
Bond strength between steel reinforcement and RCA concrete at elevated temperatures <i>Md. Abu Yusuf; Salah Sarhat; Hamzeh Hajiloo; Mark F. Green</i>	293
Evaluation of expected damage costs from fire in concrete building structures <i>Shuna Ni; Thomas Gernay</i>	301
Spalling of geopolymer concrete in ring-restrained specimens under high temperatures <i>Mitsuo Ozawa; Hiroyuki Ikeya; Koji Harada; Hiroki Goda</i>	313
Generalized fragility curves for concrete columns exposed to fire through surrogate modelling <i>Ranjit Kumar Chaudhary; Balša Jovanović; Thomas Gernay; Ruben Van Coile</i>	322
Critical fibre dimensions for preventing spalling of ultra-high performance concrete at high temperature <i>Dong Zhang; Kang Hai Tan</i>	333
Probabilistic models for thermal properties of concrete <i>Balša Jovanović; Negar Elhami Khorasani; Thomas Thienpont; Ranjit Kumar Chaudhary; Ruben Van Coile</i>	342
Effect of steel fibers on fire endurance of extruded hollow-core slabs <i>Hang T N Nguyen; Kang Hai Tan</i>	353
<b>Experimental research and any other</b>	
Retrofitting of fire damaged RC columns <i>Hemanth Kumar Chinthapalli; M. Chellapandian; Anil Agarwal; Suriya Prakash</i>	363
Developing real-time hybrid simulation to capture column buckling in a steel frame under fire <i>Ramla K Qureshi; Negar Elhami Khorasani; Mettupalayam Sivaselvan</i>	374
Thermal response and capacity of beam end shear connections during a large compartment fire experiment <i>Xu Dai; Lisa Choe; Erica Fischer; Charles Clifton</i>	386



Experimental study of concrete elements subjected to travelling fires <i>Camilo Montoya; David Lange; Cristian Maluk; Juan P. Hidalgo</i>	398
Robust circle tracking for deflection measurements in structural fire experiments <i>Felix Wiesner; Luke Bisby</i>	410
Alkali-activated sprayed concrete as a fire protection coating for tunnels inner lining: proof-of-concept study on the heat transfer <i>Anna-Lena Hammer; Christian Rhein; Thomas Rengshausen; Markus Knobloch; Götz Vollmann; Markus Thewes</i>	418
Evaluation of measuring methods for water vapor pressure in concrete at elevated temperature <i>Ye Li; Kang Hai Tan</i>	430
Travelling fire in full scale experimental building subjected to open ventilation conditions <i>Ali Nadjai; Naveed Alam; Marion Charlier; Olivier Vassart; Xu Dai; Jean-Marc Franssen Johan Sjöström</i>	439
Shear resistance of sandwich panel connection to the substructure at elevated temperature <i>Kamila Cábová; Marsel Garifullin; Ashkan Shoushtarian Mofrad; František Wald; Kristo Mela; Yvonne Ciupack</i>	451
Near-limit burning of timber material under irradiation-assisted smoldering <i>Shaorun Lin; Xinyan Huang</i>	458
Rotational ductility of steel web-flange splice connections in fire <i>Paul Akagwu; Faris Ali; Ali Nadjai</i>	468
Fire experiments inside a very large and open-plan compartment: x-TWO <i>Mohammad Heidari; Egle Rackauskaite; Matthew Bonner; Eirik Christensen; Sébastien Morat; Harry Mitchell Panos Kotsovinos; Piotr Turkowski; Wojciech Wegrzynski; Piotr Tofilo; Guillermo Rein</i>	479
Assessment of a fire damaged concrete overpass: the Verona bus crash case study <i>Roberto Felicetti</i>	492
<b>Numerical modelling</b>	
Simple calculation method for the temperature profile in a circular concrete filled steel tubular column <i>Yusuke Shintani; Takuya Kinoshita; Tomohito Okazaki; Toshihiko Nishimura; Tamotsu Takao</i>	504
Simulation of pyrolysis and combustion of pine wood using two-step reaction scheme <i>Dharmit Nakrani; Tejas Wani; Gaurav Srivastava</i>	515
A simplified representation of travelling fire development in large compartment using CFD analyses <i>Marion Charlier; Olivier Vassart; Xu Dai; Stephen Welch; Johan Sjöström; Johan Anderson Ali Nadjai</i>	526

Disproportionate collapse of steel-framed gravity buildings under fires with a cooling phase <i>Jian Jiang; Bowen Wang; Wenyu Cai; Guo-Qiang Li; Wei Chen; Jihong Ye</i>	537
Simple structural models for computational analysis of restrained columns under fire conditions <i>Pedro Dias Simão; João Paulo C. Rodrigues</i>	543
A static solver for hybrid fire simulation based on model reduction and dynamic relaxation <i>Patrick. Covi; Giuseppe Abbiati; Nicola Tondini; Oreste Salvatore Bursi; Bozidar Stojadinovic</i>	556
A thermo-mechanical stochastic damage perspective for concrete at elevated temperatures <i>Hao Zhou</i>	567
Linked CFD-thermo-mechanical simulation for virtual horizontal furnace <i>Stanislav Šulc; Kamila Cábová; Filip Zeman; Jakub Šejna; Vít Šmilauer; František Wald</i>	579
AI modelling & mapping functions: a cognitive, physics-guided, simulation-free and instantaneous approach to fire evaluation <i>M Z Naser; Haley Hostetter; Aditya Daware</i>	590
A numerical investigation of 3D structural behavior for steel-composite structures under various travelling fire scenarios <i>Zhuojun Nan; Xu Dai; Haimin Chen; Stephen Welch; Asif Usmani</i>	599
An improved implicit analysis method to model transient strain of high-strength concrete during unloading at elevated temperatures <i>Shan Li; J Y Richard Liew; Ming-Xiang Xiong</i>	611
The behaviour of bridge decks due to fire induced thermal expansion of protected stays cables <i>Panagiotis Kotsovinos; Egle Rackauskaite; Ryan Judge; Graeme Flint; Peter Woodburn</i>	622
Modelling Grenfell disaster: interactions between facades and apartments <i>Eric Guillaume; Virginie Dréan; Bertrand Girardin; Talal Fateh</i>	627
<b>Steel structures</b>	
Studies on bending strength and collapse temperature of a steel beam considering effects of steel strain rate and heating rate at elevated temperatures <i>Fuimnobu Ozaki; Takumi Umemura</i>	639
Experimental and numerical-analytical study on structural behavior of steel frames based on small-scale fire tests <i>Akinobu Takada; Tomohito Okazaki; Mami Saito</i>	650
Investigation of the performance of a novel ductile connection within bare-steel and composite frames in fire <i>Yu Liu; Shan-Shan Huang; Ian Burgess</i>	662
Behaviour of axially compressed angles and built-up steel members at elevated temperature <i>Luca Possidente; Nicola Tondini; Jean-Marc Battini</i>	673

Stability check of web-tapered steel beam-columns in fire <i>Elio Maia; Paulo Vila Real; Nuno Lopes; Carlos Couto</i>	685
Post-fire mechanical properties of TMCP high strength structural steel <i>Lin-Xin Song; Guo-Qiang Li; Qing Xu</i>	697
Prediction of fracture behavior for high-strength steel bolts at elevated temperatures <i>Wenyu Cai; Jian Jiang; Guo-Qiang Li</i>	708
New methodology for the calculations on steel columns with thermal gradients in contact with brick walls <i>António Moura Correia; João Paulo Rodrigues; Venkatesh Kodur</i>	715
OpenSees simulation of the collapse of Plasco tower in fire <i>Ramakanth Veera Venkata Domada; Aatif Ali Khan; Mustesin Ali Khan; Asif Usmani</i>	727
Fire resistance of stainless steel slender elliptical hollow section beam-columns <i>Flávio Arrais; Nuno Lopes; Paulo Vila Real</i>	739
Material properties of structural, high strength and very high strength steels for post-fire assessment of existing structures <i>Tom Molkens; Katherine A. Cashell; Barbara Rossi</i>	751
Fire fragility curves for steel pipe-racks exposed to localised fires <i>Jérôme Randaxhe; Olivier Vassart; Nicola Tondini</i>	763
A novel approach to model the thermal and physical behaviour of swelling intumescent coatings exposed to fire <i>Andrea Lucherini; Juan P. Hidalgo; Jose L. Torero; Cristian Maluk</i>	775
Experimental study of unloaded structural steel stay-cables under fire exposure <i>Benjamin Nicoletta; Scott Watson; Bronwyn Chorlton; John Gales; Panagiotis Kotsovinos</i>	783
Experimental investigation of the behavior of martensitic high-strength steels at elevated temperature <i>Xia Yan; Yu Xia; Hannah B. Blum; Thomas Gernay</i>	791
Effect of transient creep on stability of steel columns exposed to fire <i>Venkatesh Kodur; Svetha Venkatachari</i>	803
<b>Timber structures</b>	
Compressive strength and MoE of solid softwood at elevated temperatures <i>Abdulrahman Zaben; David Lange; Cristian Maluk</i>	811
A method for determining time equivalence for compartments with exposed mass timber, using iterative parametric fire curves <i>David Barber; Robert Dixon; Egle Rackauskaite; Khai Looi</i>	818

Calibration of a coupled post-flashover fire and pyrolysis model for determining char depth in mass timber enclosures <i>Colleen Wade; Danny Hopkin; Michael Spearpoint; Charles Fleischmann</i>	830
The behaviour of timber in fire including the decay phase - charring rates, char recession and smouldering <i>Joachim Schmid; Antonio Totaro; Andrea Frangi</i>	842
Design of timber-concrete composite floors for fire <i>Erica C. Fischer; Annabel B. Shephard; Arijit Sinha; Andre R. Barbosa</i>	852
Proposal for stress-strain constitutive models for laminated bamboo at elevated temperatures <i>Mateo Gutierrez Gonzalez; Cristian Maluk</i>	859
The use of research for the explicit consideration of self- extinction in the design of timber structures <i>Juan Cuevas; Cristian Maluk</i>	866
Fire performance of moment-resisting concealed timber connections reinforced with self-tapping screws <i>Oluwamuyiwa Okunrounmu; Osama (Sam) Salem; George Hadjisophocleous</i>	879
Deformation behaviour and failure time of glued laminated timber columns in fire <i>Takeo Hirashima; Heisuke Yamashita; Shungo Ishi; Tatsuki Igarashi; Shigeaki Baba; Tomoyuki Someya</i>	890
Comparative study on the fire behaviour of fire-rated gypsum plasterboards vs. thin intumescent coatings used in mass timber structures <i>Ambrosine Hartl; Qazi Samia Razzaque; Andrea Lucherini; Cristian Maluk</i>	901
The response of exposed timber in open plan compartment fires and its impact on the fire dynamics <i>Sam Nothard; David Lange; Juan P. Hidalgo; Vinny Gupta; Martyn S. McLaggan</i>	911

## BEHAVIOUR OF AXIALLY COMPRESSED ANGLES AND BUILT-UP STEEL MEMBERS AT ELEVATED TEMPERATURE

Luca Possidente<sup>1</sup>, Nicola Tondini<sup>2</sup>, Jean-Marc Battini<sup>3</sup>

### ABSTRACT

Angles and built-up steel sections are widely employed in structures as members in bracing systems or in truss structures and are mainly designed to withstand axial loads. Torsional and flexural-torsional buckling might affect angles and built-up members subjected to compressive stresses. Great interest has been shown by researchers relative to the instability of steel elements in fire, but there is a lack of studies on the buckling behaviour of angles and built-up steel members in compression and this topic is not explicitly treated in the current version of Eurocode EN 1993-1-2. In order to provide new insights, a comprehensive numerical investigation of the behaviour of concentrically compressed angles, tee and cruciform steel members at elevated temperature was performed. A parametric study was carried out on Class 1 to 3 profiles with three different steel grades, namely S235, S275, S355, subjected to uniform temperature distribution. More than 41000 geometrically and materially nonlinear imperfect analyses (GMNIA) were performed on columns with different length and temperature by means of 3D beam and shell elements. Results showed that the buckling curve given in EN 1993-1-2 provides unconservative predictions for a range of slenderness of practical interest. To better predict the behaviour of the investigated steel members, an improved buckling curve was proposed, which allows for safer predictions, as also confirmed by statistical investigation.

**Keywords:** Steel structures; Flexural-torsional buckling; Torsional buckling; Fire; finite element modelling; Buckling curve

### 1 INTRODUCTION

Steel angular, cruciform and tee sections are frequently employed in bracing systems or in truss structures, in which they are mainly axially loaded. Thus, when subjected to compressive actions their resistance can be affected by instability phenomena. Local effects are negligible for compact sections and global buckling modes govern the behaviour of the steel elements. Unless flexural buckling is prevented by lateral restraints, in typical hot-rolled or welded I or H profiles that are axially compressed, torsional effects are rare. However, for angles, tee and cruciform steel sections, torsional or flexural-torsional buckling can be relevant, in particular, in a low slenderness range. Hereafter angles, tee and cruciform sections are referred to as L, T and X sections respectively. Prescriptions for the design of compressed steel members at both ambient and elevated temperature are given in EN 1993-1-1 [1] and EN 1993-1-2 [2], respectively. The resistance is reduced according to the slenderness of the element and buckling curves are provided. These curves were based on experimental and numerical results for H- and I-profiles and later, were calibrated

---

<sup>1</sup> PhD student, University of Trento; Department of Civil, Environmental and Mechanical Engineering, Via Mesiano 77, 38123, Trento, Italy & KTH, Royal Institute of Technology - Department of Civil and Architectural Engineering, SE-10044 Stockholm, Sweden  
e-mail: luca.possidente@unitn.it, ORCID: <https://orcid.org/0000-0002-4179-1860>

<sup>2</sup> Assistant Professor, University of Trento; Department of Civil, Environmental and Mechanical Engineering, Via Mesiano 77, 38123, Trento, Italy  
e-mail: nicola.tondini@unitn.it

<sup>3</sup> Professor, KTH, Royal Institute of Technology - Department of Civil and Architectural Engineering, SE-10044 Stockholm, Sweden  
e-mail: jean-marc.battini@byv.kth.se

and extended to other profiles, such as L profiles. In EN 1993-1-2 [2] flexural buckling is considered according to the model presented by Franssen et al. [3]. Then, researchers investigated the effects of other instability phenomena on the resistance of steel elements at elevated temperature such as lateral-torsional buckling [4]-[6] and its interaction with local instabilities [7]-[11]. However, axially compressed steel members in fire may be also prone to torsional and flexural-torsional buckling. Such buckling phenomena have been particularly studied for cold-formed steel profiles at both ambient and elevated temperatures [12]-[16]. Indeed, owing to the shape and the small thickness, an interaction of local, distortional and global buckling influences the resistance of L, T and X thin-walled members at ambient temperature, as shown by Dinis et al. [17]. Further considerations on X sections were provided in [18]-[20]. The work presented in this paper aims at providing indications about the torsional and flexural-torsional buckling of compressed L, T and X steel profiles, obtained by coupling L sections or by cutting H or I hot rolled profiles. Dedicated buckling curves were proposed based on the results of a numerical investigation. Statistical investigation was employed to compare the proposed model and the one prescribed in EN 1993-1-2 [2].

## 2 EUROCODE PROVISIONS

The resistance of steel members should be reduced to account for the effect of temperature. According to EN 1993-1-2 [2], for compressed elements with a uniform temperature  $\theta_a$  and Class 1, Class 2 or Class 3 cross-sections, the resistance is determined as follows:

$$N_{b,fi,t,Rd} = \frac{\chi_{fi} A k_{y,\theta} f_y}{\gamma_{M,fi}} \quad (1)$$

where  $\gamma_{M,fi}$  is the safety factor for the fire design situation,  $A$  is the area of the cross-section,  $k_{y,\theta}$  is the retention factor for the yield strength of steel at temperature  $\theta_a$  and  $f_y$  is the yield strength.  $\chi_{fi}$  is the flexural buckling coefficient in the fire design situation, and is obtained according to the following equation:

$$\chi_{fi} = \frac{1}{\varphi_{\theta} + \sqrt{\varphi_{\theta}^2 - \bar{\lambda}_{\theta}^2}} \quad (2)$$

with

$$\varphi_{\theta} = \frac{1}{2} \left[ 1 + \eta_{EC3.1-2} + \bar{\lambda}_{\theta}^2 \right] \quad (3)$$

The generalised imperfection factor  $\eta_{EC3.1-2}$  is defined as

$$\eta_{EC3.1-2} = \alpha \bar{\lambda}_{\theta} \quad (4)$$

the imperfection factor  $\alpha$  depends on the yield strength  $f_y$  expressed in MPa

$$\alpha = \beta \sqrt{\frac{235}{f_y}}; \quad \beta = 0.65 \quad (5)$$

While the non-dimensional slenderness  $\bar{\lambda}_{\theta}$  at the temperature  $\theta_a$ , is given by:

$$\bar{\lambda}_{\theta} = \bar{\lambda} \left[ \frac{k_{y,\theta}}{k_{E,\theta}} \right]^{0.5} \quad (6)$$

$k_{y,\theta}$  and  $k_{E,\theta}$  are the reduction factors for the yield strength and Young's modulus at steel temperature  $\theta_a$ ,  $\bar{\lambda}$  is the non-dimensional slenderness at ambient temperature. Further explanations about the design procedure and the definition of  $\bar{\lambda}$  are not provided in the code for steel structures in fire situation. Instead, the definition of the non-dimensional slenderness at ambient temperature can be found in EN 1993-1-1 [1], which prescribes that for Class 1, 2 and 3 cross-sections at ambient temperature  $\bar{\lambda}$  is determined as follows

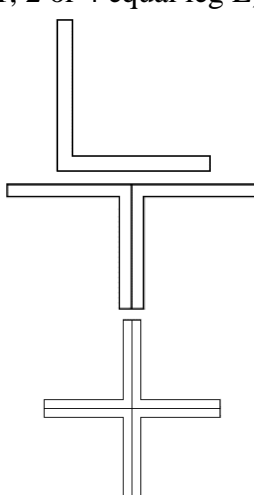
$$\bar{\lambda} = \bar{\lambda}_{cr} = \sqrt{\frac{A f_y}{N_{cr}}} \quad (7)$$

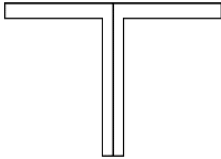
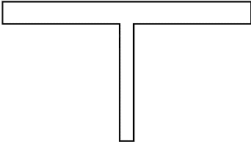
$N_{cr}$  is the lowest elastic critical load at ambient temperature. Hence, the slenderness  $\bar{\lambda}$  is associated with the lowest relevant buckling mode, that in some cases might be torsional or flexural-torsional. However, in EN 1993-1-2 [2]  $\chi_{fi}$  is defined as the smaller between the flexural buckling coefficients  $\chi_{y,fi}$  and  $\chi_{z,fi}$ , and thus, flexural-torsional buckling is not considered. The two different approaches might be in contrast and lead to confusion. Indeed, following the philosophy of EN 1993-1-2 [2],  $N_{cr}$  should be defined as the lowest pure flexural mode ( $N_{cr,F} = \min(N_{cr,y}, N_{cr,z})$ ) but, in order to account for torsional effects, the value of  $N_{cr}$  associated to the lowest relevant buckling mode should be employed as in prescribed EN 1993-1-1 [1].

### 3 PARAMETRIC ANALYSIS

The behaviour of concentrically compressed members subjected to fire that may be sensitive to torsional or flexural-torsional buckling was investigated, performing a large number of Finite Element Analysis (FEA). Results in terms of resistance were compared with the EN 1993-1-2 provisions, and the accuracy and safety of the predictions were discussed. The analysed members consisted of L, T or X cross-sections, defined by coupling L sections back-to-back in case of T and X sections or by cutting in two halves H or I hot rolled steel profiles for additional T sections. In the case of coupled sections, it was assumed that, if the spacing of the connections is short enough, closely built-up members can be checked for buckling as single integral members [1]. Meaningful predictions of the behaviour of coupled members were obtained with this assumption in several papers [17]-[20]. Nevertheless, connecting plates or battens could be considered in more refined numerical models. 3D beam and shell elements were used in more than 41000 geometrically and materially imperfect nonlinear analyses (GMNIA). The length and the temperature of the columns were varied. Columns subjected to five different uniform temperatures were studied: 400°C, 500°C, 600°C, 700°C, 800°C. The temperature range 400°C-800°C is the most relevant temperature range for columns subjected to uniform temperature. This was proved for columns that buckle flexurally [3] and preliminary analyses showed that it holds true for the cross-sections studied in this work. For each temperature about 8200 columns were analysed with a length-to-width ratio higher than 3, in order to limit the analyses to columns of practical interest. 45 different equal leg L profiles of commercial dimensions were studied. 68 T section and 45 X sections were obtained by coupling 2 and 4 L sections respectively. 129 T sections were obtained by dividing into two halves hot rolled H- or I-sections. The different section types are summarised in Table 1. Classes in fire situation were defined according to EN 1993-1-2 [2] and the steel grade of each column was selected so that only cross-sections of Class 1, Class 2 or Class 3 were investigated.

Table 1. Investigated sections - •S235; #S275; +S355

Section type	Dimensions of the angles composing the sections (Flange depth x web height x flange thickness x web thickness in mm)			
	45x45x7x7	#+	150x150x20x20	• +
	50x50x9x9	#+	150x150x18x18	•#
	60x60x10x10	#+	160x160x17x17	•
	65x65x11x11	+	180x180x19x19	•
	65x65x10x10	#+	200x200x28x28	#+
	70x70x9x9	#+	200x200x26x26	•#+
	90x90x16x16	•#+	250x250x34x34	#+
	100x100x16x16	•#+	250x250x33x33	#+
	100x100x15x15	•#+	250x250x32x33	+
	110x110x12x12	•	250x250x27x27	•
	120x120x15x15	•#	300x300x33x33	•
	120x120x13x13	•	300x300x32x32	•
	140x140x16x16	•#		

T sections (2 unequal leg L) 	65x100x9x9	•	90x130x12x12	•		
	65x100x10x10	•#	90x130x14x14	•#+		
	65x100x12x12	•#+	90x140x12x12	•		
	70x110x10x10	•#	90x140x14x14	•#		
	70x110x12x12	•#+	100x150x14x14	•#		
	80x120x12x12	•#	100x200x16x16	•		
T sections (half H or I) 		<i>From half</i>		<i>From half</i>		
	120x54,5x4,2x5,5	HE 120 AA	•#+	248x135x18x32	HE 240 M	•#+
	120x57x5x8	HE 120 A	•#+	280x140x10,5 x18	HE 280 B	•#+
	64x60x4,4x6,3	IPE 120	#+	268x145x18x32,5	HE 260 M	•#+
	120x60x6,5x11	HE 120 B	•#+	300x150x11x19	HE 300 B	•#+
	140x64x4,3x6	HE 140 AA	#+	288x155x18,5 x33	HE 280 M	•#+
	140x66,5x5,5x8,5	HE 140 A	•#+	300x160x11,5x20,5	HE 320 B	#+
	126x70x12,5x21	HE 120 M	•#+	310x170x21x39	HE 300 M	•#+
	140x70x7x12	HE 140 B	•#+	300x170x12x21,5	HE 340 B	#+
	160x74x4,5x7	HE 160 AA	+	309x179,5x21x40	HE 320 M	•#+
	160x76x6x9	HE 160 A	•#+	300x180x12,5x22,5	HE 360 B	#+
	146x80x13x22	HE 140 M	•#+	309x188,5x21x40	HE 340 M	•#+
	160x80x8x13	HE 160 B	•#+	308x197,5x21x40	HE 360 M	•#+
	180x85,5x6x9,5	HE 180 A	#+	300x200x13,5x24	HE 400 B	+
	166x90x14x23	HE 160 M	•#+	307x216x21x40	HE 400 M	•#+
	180x90x8,5x14	HE 180 B	•#+	307x239x21x40	HE 450 M	•#+
	200x95x6,5x10	HE 200A	#+	306x262x21x40	HE 500 M	•#+
	186x100x14,5x24	HE 180M	•#+	306x286x21x40	HE 550 M	#+
	200x100x9x15	HE 200B	•#+	305x310x21x 40	HE600M	#+
	220x105x7x11	HE 220A	#+	310x316x25,5x46	HE600x337	•#+
	206x110x15x25	HE 200M	•#+	315x324x30x54	HE600x399	•#+
	220x110x9,5x16	HE 220B	•#+	309x340x25x46	HE650x343	#+
	240x115x7,5x12	HE 240A	#+	314x348x29,5x54	HE650x407	•#+
	226x120x15,5 x26	HE 220M	•#+	308x364x25x46	HE700x352	+
	240x120x10x17	HE 240B	•#+	313x372x29,5 x54	HE700x418	#+
	260x125x7,5x12,5	HE 260A	+	313x421x30x54	HE800x444	+
	260x130x10x17,5	HE 260 B	•#+			

### 3.1 Finite element modelling

Linear eigenvalue analyses were performed to determine the shape of the initial geometric imperfection to be introduced in each analysis. These imperfections were scaled so that the maximum nodal displacement along the column equalled 1/1000 of the length. The elasto-plastic behaviour of steel was modelled based on the Von Mises yield function and on the uniaxial stress-strain relationship given in EN 1993-1-2 [2]. Residual stresses were neglected since it was found that their effect on the resistance of steel member in fire is not significant [3], [7], [15], [24], [25]. Three steel grades were selected, i.e. namely S235, S275, S355. The Young's modulus value at ambient temperature was set to 210 GPa and the Poisson ratio was equal to 0.3. The monosymmetric sections (L and T sections) were investigated by means of the 3D beam finite elements developed in [22], whereas for the X section the shell element proposed in [23] was



employed. Indeed, shell elements were used as the introduction of imperfections associated to a pure torsional buckling would not be possible in beam elements-based analyses. However, beam elements were preferred for the monosymmetric cross-sections since they enable faster analyses and an easier definition of the boundary conditions, allowing for the investigation of simply supported columns, with the rotational degree of freedom along the longitudinal axis blocked. Instead, columns with clamped end conditions were analysed when shell elements were used. In detail, the lateral displacements were blocked only at the centroids of the two clamped ends, to allow for thermal expansion. The axial displacement was fixed on one end and free conditions were imposed at the opposite one, which was loaded. The axial load was applied to the centroid and master-slave constraints allowed for a uniform axial displacement of all the other nodes of the loaded end. Preliminary convergence analyses showed that 30 elements were sufficient for accurate solutions regarding beam models, while in the shell-based simulation it was necessary to vary the mesh with the length of the column. A minimum of 6 elements in each dimension of the section were always used.

### 3.2 Validation of the numerical models

The ability of beam and shell models to capture flexural-torsional buckling was validated numerically, since no experimental tests were available in literature. The behaviour of a compressed T section consisting of two 150x150x20x20 L sections (see Table 1) at elevated temperature was studied by means of both the shell and beam elements. Both ends of the column were clamped, except for the axial displacement that was free on the loaded side. In order to study a column that exhibits flexural-torsional behaviour, the length of the column was set to  $L=1.67$  m. This was confirmed by a linear buckling analysis at ambient temperature, which identified flexural-torsional buckling as the lowest buckling mode for both the shell and the beam models (see Figure 1a). In terms of the associated buckling loads, a difference of only 3.2% was registered between the analyses ( $N_{cr,BEAM}=12150$  kN and  $N_{cr,SHELL}=12550$  kN). Then, the column was studied under a uniform and constant temperature of  $600^{\circ}\text{C}$  and an increasing compressive load  $N$ . The buckling mode shapes obtained in the previous linear buckling analyses were scaled and introduced as initial geometric imperfection in the numerical models. Figure 1b shows the load-displacement path of the loaded node. The load  $N$  is expressed with respect to the yield load  $N_{yield} = Ak_{y,600^{\circ}\text{C}}f_y$ . The results are in excellent agreement with the outcomes of the same analysis performed with a shell model developed in SAFIR [37]. An almost identical load level with a maximum difference of 3.7% was achieved.

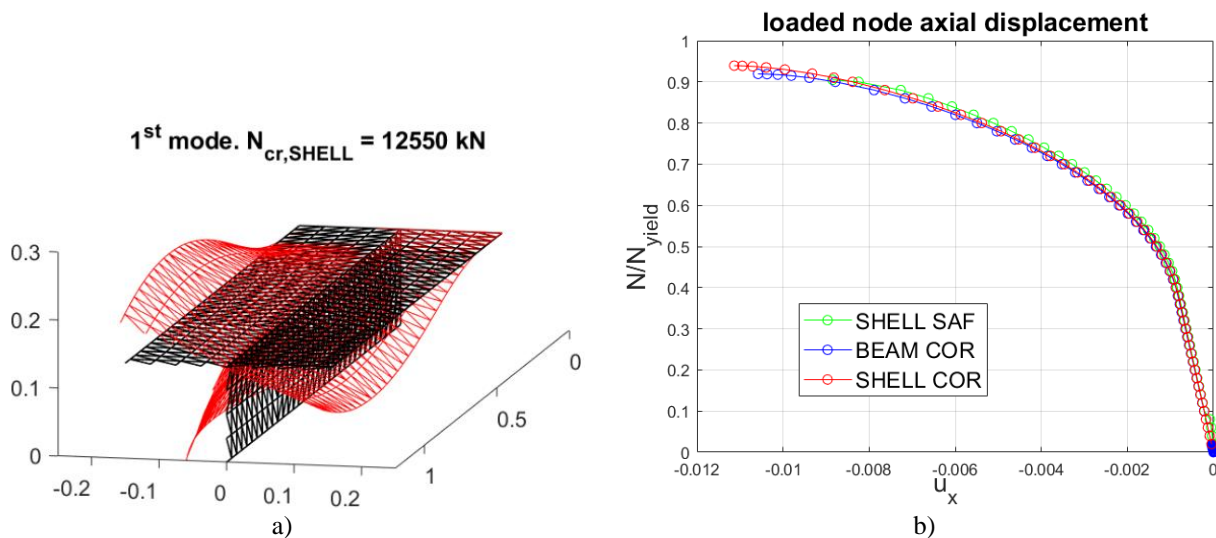


Figure 1. Validation test. Lowest buckling mode of the shell analysis; b) Load vs axial displacement of the loaded node

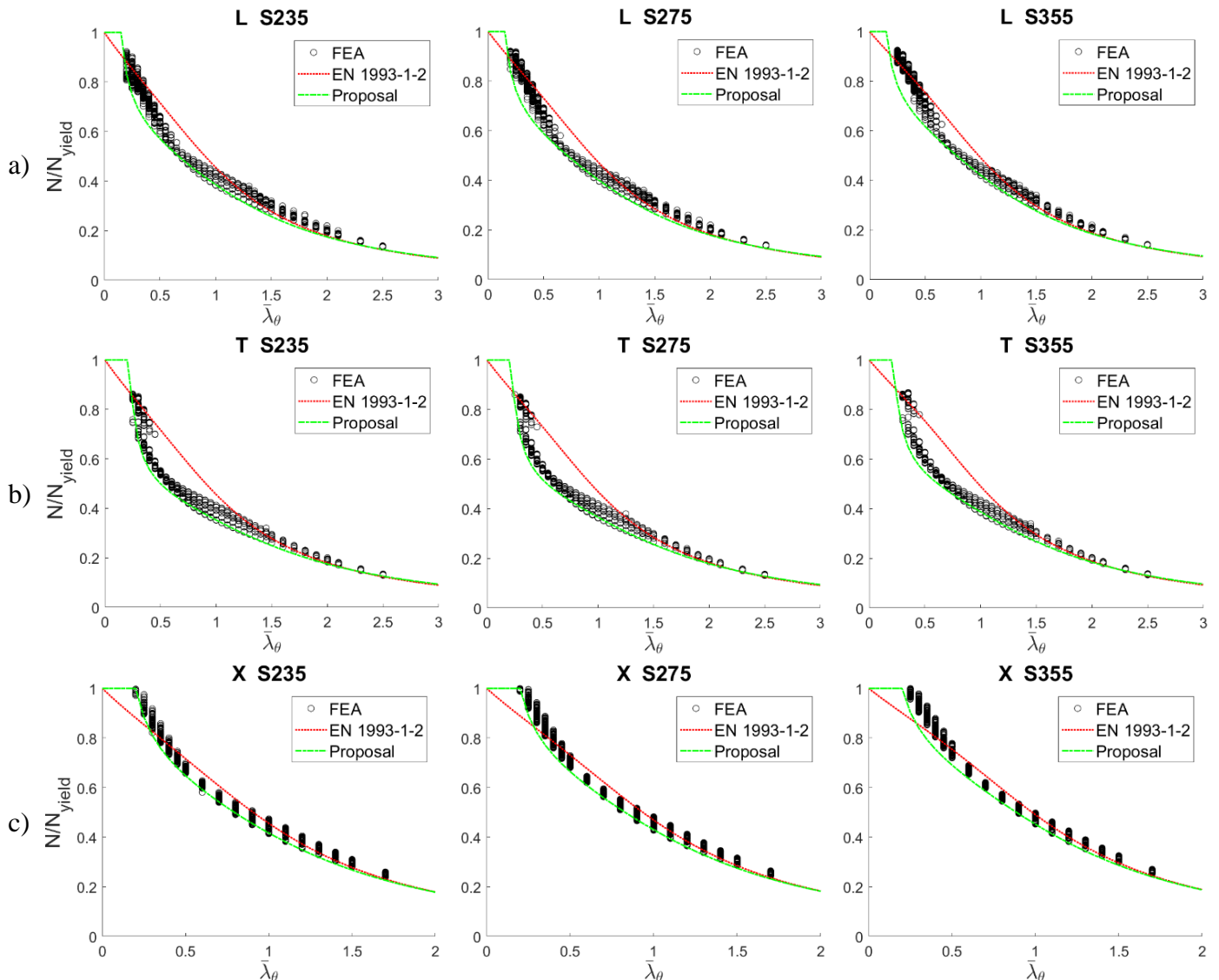
### 3.3 Description and discussion of the numerical results

The numerical outcomes of the parametric analysis are illustrated in Figure 2, where the numerical failure load  $N$  is expressed with respect to the yielding load at elevated temperature  $N_{yield} = Ak_{y,\theta}f_y$  in order to compare the numerical outcomes with the buckling coefficient  $\chi_{fi}$  from EN 1993-1-2 [2]. Since it was

found that a better representation of the results is obtained with buckling curves expressed with respect to the pure flexural buckling slenderness,  $\bar{\lambda}$  in Eq. (6) was defined as follows

$$\bar{\lambda} = \bar{\lambda}_{cr,F} = \sqrt{\frac{Af_y}{N_{cr,F}}} = \sqrt{\frac{Af_y}{\min(N_{cr,y}, N_{cr,z})}} \quad (8)$$

Where  $\bar{\lambda}_{cr,F}$  instead of  $\bar{\lambda}_{cr}$  was used. Analogously, Taras and Greiner [21] and Popovic et al. [14] observed that when the torsional or flexural-torsional mode is the relevant lowest buckling mode, the length of a column  $l$  may not be well represented by the non-dimensional slenderness  $\bar{\lambda}_{cr}$ . Figure 2 shows that the actual design buckling curve well represents the numerical results and provides safe predictions only for very slender columns ( $\bar{\lambda}_\theta > 1.5$ ). For all the sections and steel grades the buckling coefficient  $\chi_{fi}$  ( $=N/N_{yield}$ ) is overestimated for a medium slenderness range, in particular in the range  $0.4 \leq \bar{\lambda}_\theta < 1.2$ , in which the load-bearing capacity obtained with the EN 1993-1-2 buckling curves attain values significantly higher than the ones from the numerical simulation. Over-conservative predictions might be obtained for very stocky columns. Results for stocky columns with T sections obtained from dividing into two halves a H or I section are more spread, and the actual buckling curve is both conservative and non-conservative. However, since it seems difficult to obtain very accurate predictions in this case, a buckling curve on the safe side should be preferred. Summarising, for a large slenderness range of practical interest the buckling curve from EN 1993-1-2 provides inaccurate and non-conservative results. It would be beneficial to provide a different formulation for buckling curves, to improve the accuracy and safety of the predictions.



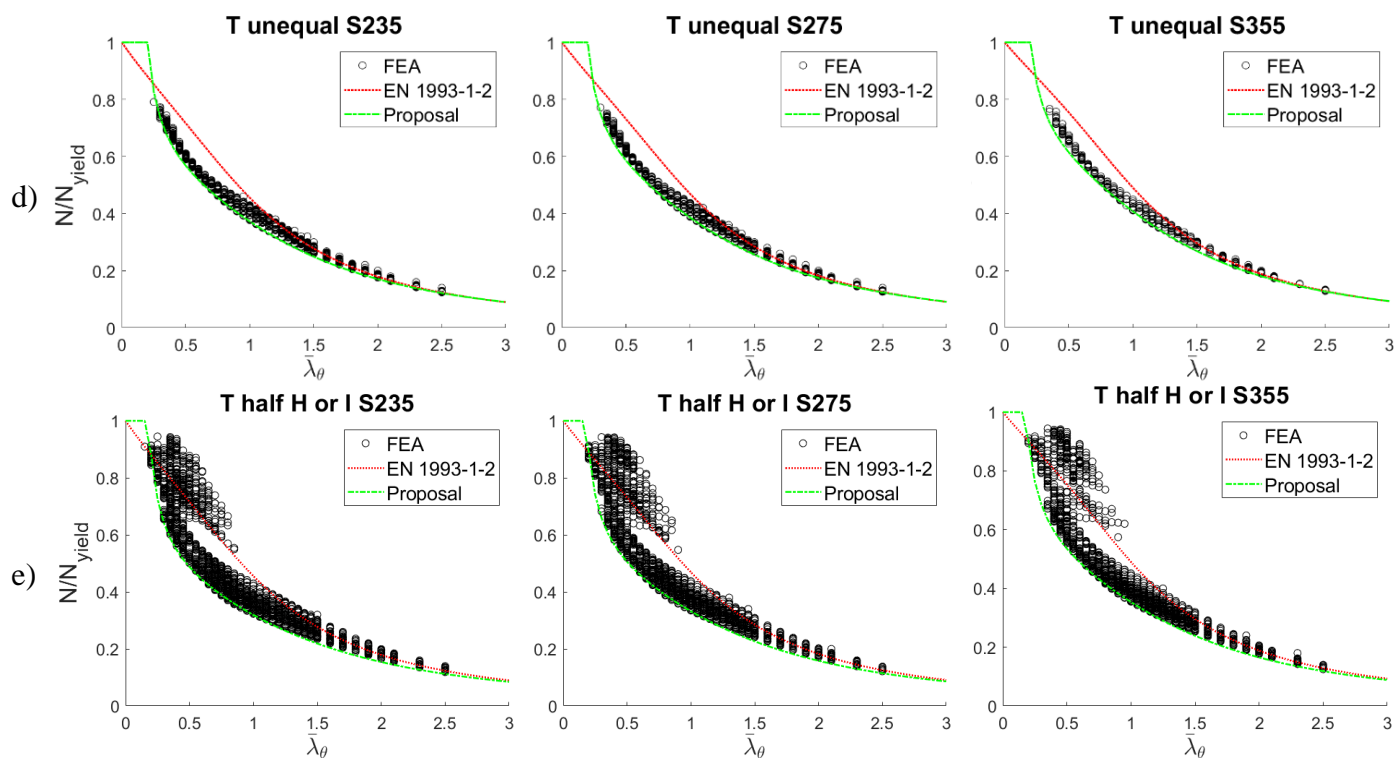


Figure 2. Buckling curves for S235, S275 and S355 steel grade. a) L, b) T and c) X made of coupled equal leg L sections, d) T obtained from unequal leg L sections and e) T obtained from half H or I section

It should be noted that in almost all the analyses of the X sections buckling occurred in its pure flexural form. Moreover, few very stocky columns attained failure loads higher than the yielding load ( $N > N_{yield}$ ) and the associated results are not shown in Figure 2, as they would imply buckling coefficients  $\chi_{fi} > 1$ , while  $\chi_{fi}$  should never exceed the value of 1. Failure loads exceeding the yielding load in shell analyses were also found in several works about the fire behaviour of steel elements subjected to lateral-torsional buckling and of cold-formed steel beams with open cross-sections [8]-[10], [16].

T sections obtained from hot-rolled H or I profiles need a separate discussion since, as evident from Figure 2, numerical results are more spread compared with the ones of the other sections. This is mainly due to the fact that these sections have very different geometric dimension, especially when it comes to the depth-to-thickness ratio of the flanges and of the web. Moreover, in some cases the strong axis of the section is directed along the web, but in the others, it has the same orientation of the flanges. This is not the case for T sections obtained by coupling L profiles. Indeed, coupling equal leg profiles the strong axis is always directed along the web, while for T sections obtained by coupling unequal leg profiles the strong axis is directed along the flange. A further difference consists in the fact that in sections obtained from H- or I-profiles, the web thickness is smaller than the flange thickness, while for the other T sections, the web thickness is always two times the flange thickness.

#### 4 NEW BUCKLING CURVE PROPOSAL

Buckling curves that allow for a better representation of the results of numerical simulation were defined, based on the curves provided in EN 1993-1-2 [2]. In detail, to improve the buckling curve formulation it was decided to modify the generalised imperfection factor  $\eta$  by embracing the same philosophy of the buckling curves as defined in EN 1993-1-1 [1] and in EN 1993-1-2 [2]. The generalised imperfection factors for the different curves are summarised in Table 2.

Table 2. Generalised imperfection factors. EN 1993-1-1 [1], EN 1993-1-2 [2] and proposal

$\eta_{EC3.1-1}$	$\eta_{EC3.1-2}$	$\eta_{PROP}$
$\alpha(\bar{\lambda} - \bar{\lambda}_0)$	$\alpha\bar{\lambda}_\theta$	$\frac{\alpha}{\bar{\lambda}_\theta^\gamma} \left( \bar{\lambda}_\theta - \frac{\bar{\lambda}_0^2}{\bar{\lambda}_\theta} \right)$

The new generalised imperfection factor  $\eta_{PROP}$  introduces a plateau up to slenderness  $\bar{\lambda} = \bar{\lambda}_0$ , while the shape of the curve depends on the parameters  $\gamma$  and  $\alpha$ . The imperfection factor  $\alpha$  is defined according to Eq. (5) and thus, the parameters  $\beta$ ,  $\gamma$  and  $\bar{\lambda}_\theta$  allow for the complete description of the buckling curve. Since a plateau was introduced, Eq. (2) should be replaced by

$$\chi_{fi} = 1 \quad \bar{\lambda}_\theta \leq \bar{\lambda}_0$$

$$\chi_{fi} = \frac{1}{\varphi_\theta + \sqrt{\varphi_\theta^2 - \bar{\lambda}_\theta^2}} \quad \bar{\lambda}_\theta > \bar{\lambda}_0 \quad (9)$$

The values of  $\beta$ ,  $\gamma$  and  $\bar{\lambda}_0$  were calibrated to propose curves on the safe side. The selected values are given in Table 3. The obtained buckling curves are compared with numerical results and the EN 1993-1-2 buckling curve in Figure 2. Predictions from the proposal are safer and the introduction of a plateau ( $\bar{\lambda}_0$ ) together with the change of the shape of the curve ( $\beta$  and  $\gamma$ ), allow for a better representation of the numerical outcomes.

Table 3. Selected values for the parameters of the proposed buckling curve

	L	T (2 equal leg L)	T (2 unequal leg L)	T (half H or I)	X (4 equal leg L)
$\beta$	1.00	1.25	1.10	1.50	0.85
$\gamma$	0.50	0.80	0.50	0.50	0.35
$\bar{\lambda}_0$	0.15	0.22	0.20	0.18	0.20

In order to provide safe predictions, an additional check on the generalised imperfection factor was performed. For this purpose, the data relative to the envelope of the minimum values of the numerical results  $N_{FEA}/N_{yield}$  in Figure 2 were selected. An equivalent numerical generalised imperfection factor  $\eta_{FEA}$  was obtained from these data and compared with  $\eta_{EC3.1-2}$  and  $\eta_{PROP}$ . Since the actual and the proposed buckling curves all derive from the equations in the following form

$$\chi_{fi} + \eta \frac{\chi_{fi}}{1 - \chi_{fi} \bar{\lambda}_\theta^2} = 1 \quad (10)$$

the imperfection factor  $\eta_{FEA}$  was obtained by substituting the reduction factor at elevated temperature  $\chi_{fi}$  with the one obtained from the data relative to the envelope of the minimum values of the numerical results  $\chi_{fi,FEA} = N_{FEA}/N_{yield}$  in Eq. (10). Hence, it holds

$$\eta_{FEA} = \left( \frac{1}{\chi_{fi,FEA}} - 1 \right) \left( 1 - \chi_{fi,FEA} \bar{\lambda}_\theta^2 \right) \quad (11)$$

In Figure 3 the generalised imperfection factors over the slenderness are compared for L sections with a steel grade of 235 MPa. Generalised factors  $\eta$  higher than  $\eta_{FEA}$  entail safe results for the design curves. Since the generalised imperfection factor  $\eta_{EC3.1-2}$  is proportional to the slenderness  $\bar{\lambda}_\theta$  it does not represent well the non-linear behaviour exhibited by  $\eta_{FEA}$ . Conversely, the  $\eta_{PROP}$  factor is in good agreement with the  $\eta_{FEA}$  for slenderness lower than 1. Better agreement could be found for higher slenderness by introducing further terms in the expression of  $\eta_{PROP}$ , but this would introduce an unnecessary complexity in the model. In fact, the higher the slenderness, the lesser the difference between the generalised

imperfection factor  $\eta$  and  $\eta_{FEA}$  affects the buckling coefficient  $\chi_{fi}$ . This is confirmed in Figure 2, in which for slenderness higher than 2, the actual and the proposed buckling curve are almost superimposed, though their generalised imperfection values are significantly different in Figure 3. Similar considerations can be drawn for all the section types and steel grades.

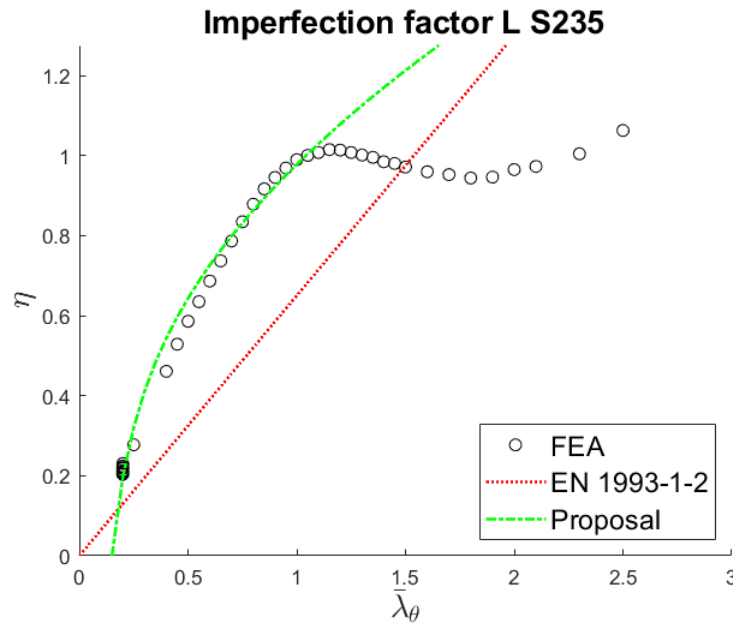
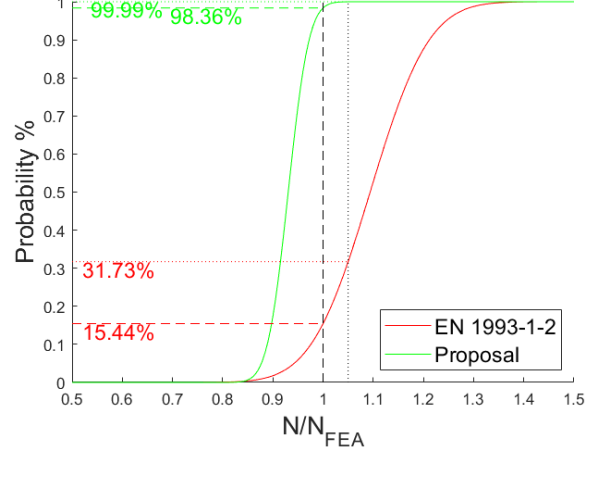
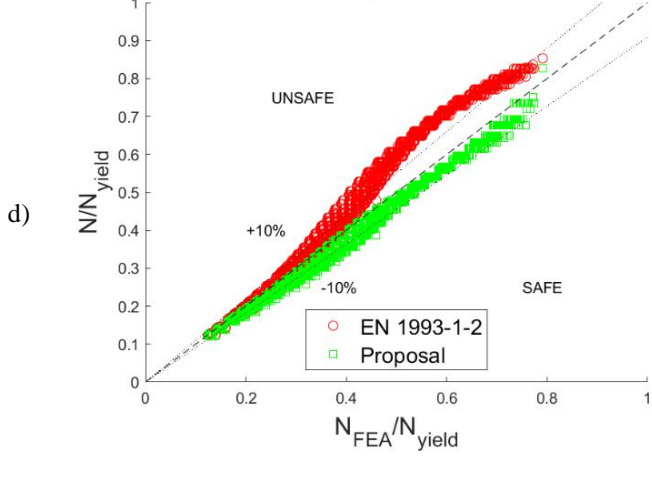
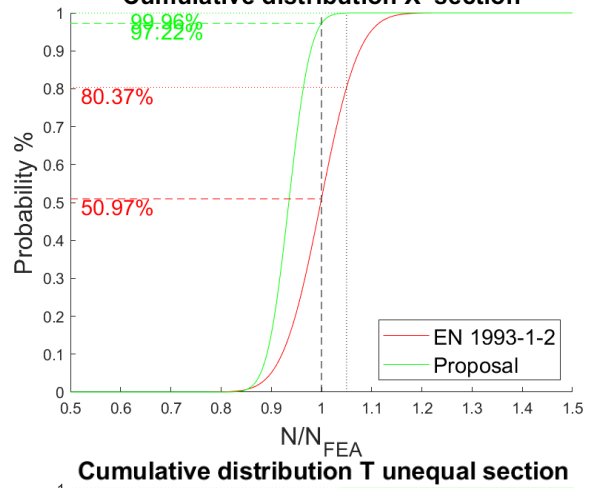
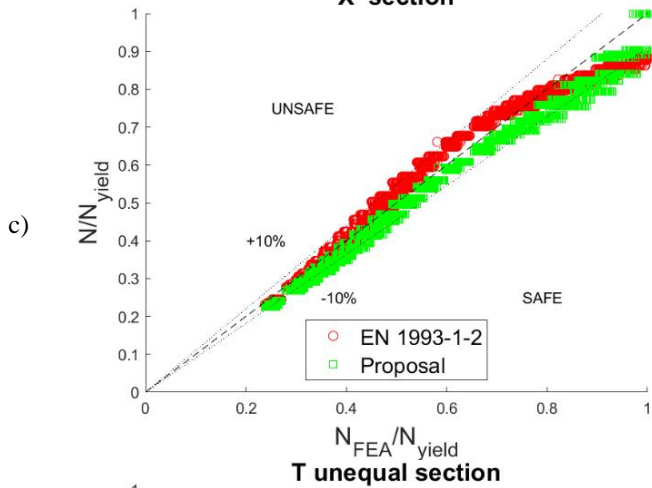
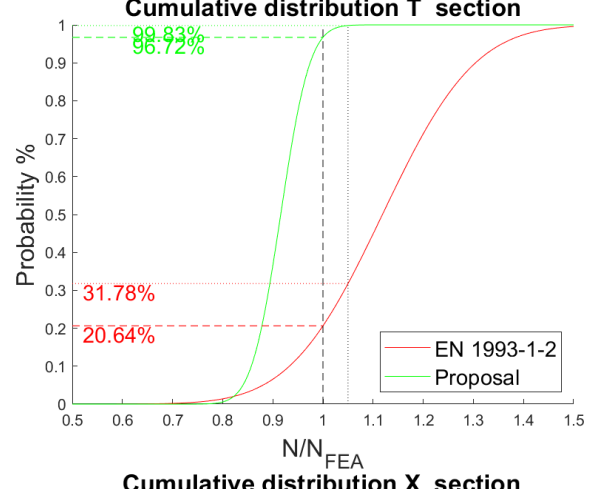
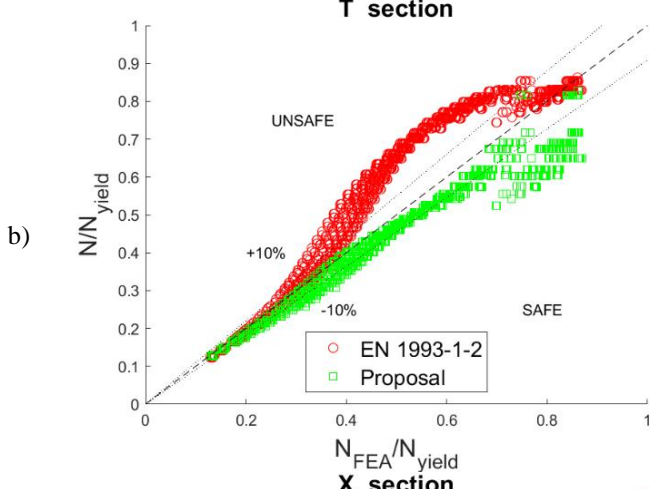
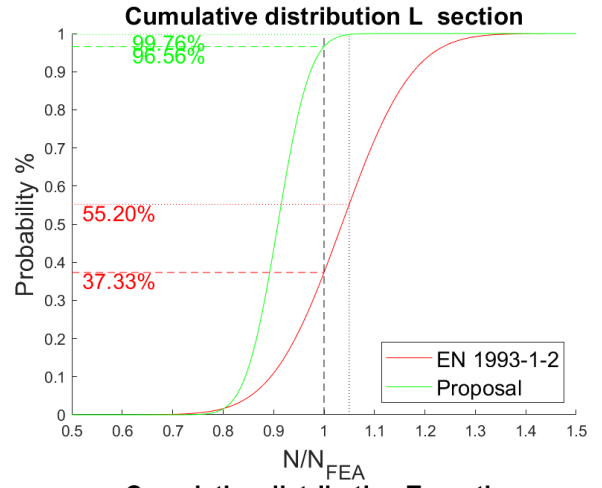
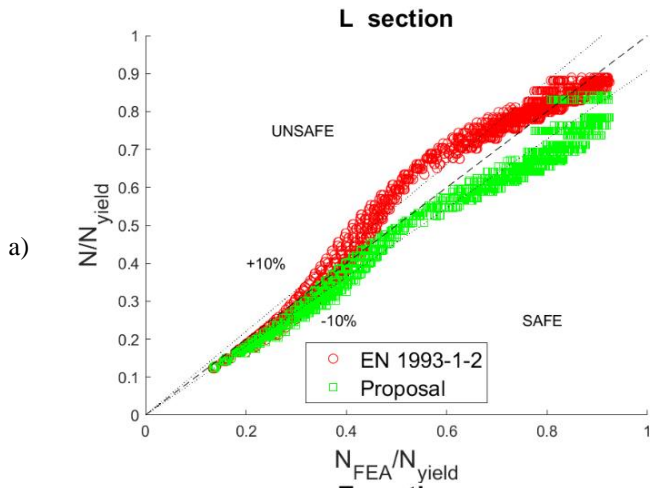


Figure 3. Generalised imperfection factors: evolution with the relative slenderness at elevated temperature for L sections and steel S235

#### 4.1 Statistical analysis

The degree of safety of the buckling curves was assessed by comparison with the results from numerical simulation. For each non-dimensional slenderness  $\bar{\lambda}_\theta$  employed in the numerical analyses, the predictions from the buckling curves were plotted against the numerical failure load  $N_{FEA}$  (Figure 4). The loads were normalised by means of the yield load  $N_{yield}$ . In Figure 7, the safe-unsafe limit is identified by the first quadrant bisector line ( $N = N_{FEA}$ ). The EN 1993-1-2 design buckling attains values significantly higher than the ones from the numerical simulation (>10%). Conversely, the proposed buckling curve is safer, and results are better distributed along the bisector line direction, especially for sections made of single or coupled L sections. The results of a statistical investigation are also presented in Figure 4, in which the safe-unsafe limit is drawn at  $N/N_{FEA} = 1$  and data are shown assuming a normal distribution. Lower standard deviations and higher frequency were obtained for the proposal. The proposal provides a probability of safe predictions higher than 96% for sections made of single or coupled L sections, and higher than 94% for the T sections obtained from half H or I section. These probabilities of non-exceedance of the safe-unsafe limit are significantly higher compared to the ones from the EN 1993-1-2 design curve. Introducing a safety margin of 5% the probabilities of non-exceedance raise to more than 98%.



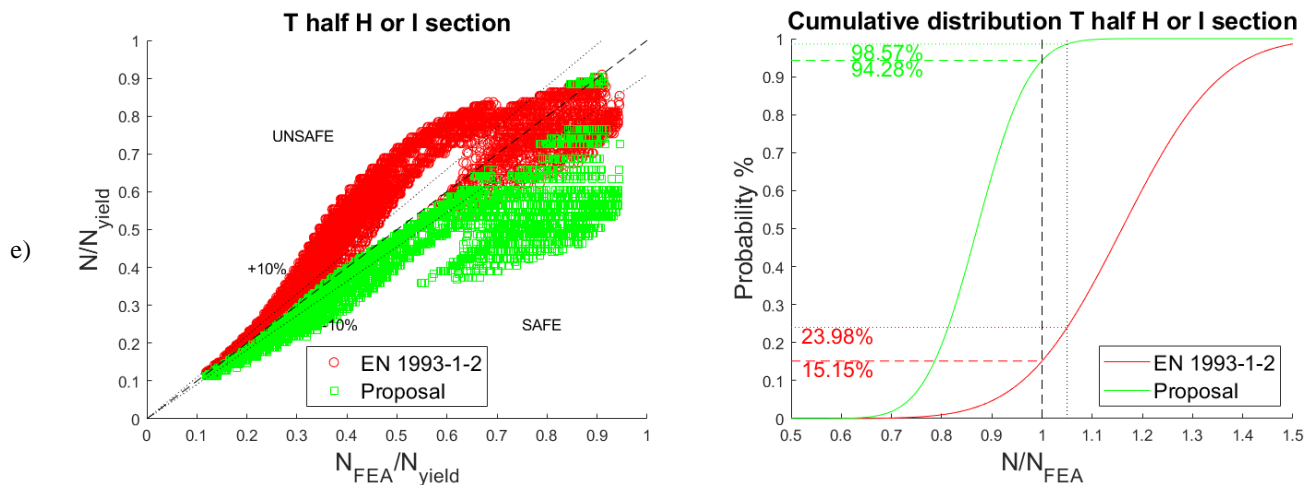


Figure 4. Numerical results vs predictions and statistical investigation. a) L, b) T and c) X made of coupled equal leg L sections, d) T obtained from unequal leg L sections and e) T obtained from half H or I section

## 5 CONCLUSIONS

A parametric analysis consisting of more than 41000 analysis was carried out to investigate the behaviour of axially compressed steel elements prone to torsional and flexural-torsional buckling at elevated temperature. It was found that flexural and flexural-torsional buckling may affect the resistance to compression of L, T and X sections in fire situation in the low slenderness range. Compared with numerical outcomes, the actual provisions of EN 1993-1-2 lead to both conservative and unconservative predictions. In detail, for a large range of medium slenderness, i.e.  $0.4 \leq \bar{\lambda}_\theta < 1.2$ , the load-bearing capacity is significantly overestimated by the EN 1993-1-2 buckling curve. In order to obtain safer and more reliable predictions, a new buckling curve was proposed. The latter differs from the formulation provided in EN 1993-1-1 and EN 1993-1-2 only in the definition of the generalised imperfection factor  $\eta_{PROP}$ , which is determined by three parameters, namely  $\beta$ ,  $\gamma$  and  $\bar{\lambda}_\theta$ . The values assumed by these parameters were given for each investigated cross-section shape. The proposal was shown to be safer and more accurate. A statistical investigation was performed as well, and assuming a normal distribution, probabilities of safe predictions higher than 94% were reached. For T sections obtained from half an H or I section, the proposal was less accurate, but still safer and more reliable than the EN 1993-1-2 curve. It was found that a better representation of the results was obtained with buckling curves expressed with respect to the pure flexural buckling slenderness because the length of a column  $l$  may not be well represented by the non-dimensional the torsional or flexural-torsional slenderness. In future research, more refined finite element models could be employed to account for the influence of connecting plates or battens in elements made of coupled L sections. Moreover, experimental investigation would be beneficial.

## ACKNOWLEDGMENTS

The authors acknowledge funding from the Italian Ministry of Education, University and Research (MIUR) in the frame of the Departments of Excellence Initiative 2018–2022 attributed to DICAM of the University of Trento

## REFERENCES

1. European Committee for Standardisation (2005). Eurocode 3 Design of steel structures - Part 1-1: General rules and rules for buildings.
2. European Committee for Standardisation (2005). Eurocode 3 Design of steel structures - Part 1-2: General rules - Structural fire design
3. J.-M. Franssen, J.-B. Schleich, L.-G. Cajot (1995). A simple Model for the Fire Resistance of Axially-loaded Members According to Eurocode 3. Journal of Constructional Steel Research, Vol 35, pp. 49-69.

4. C.G. Bailey, I.W. Burgess, R.J. Plank, The lateral-torsional buckling of unrestrained steel beams in fire, *J. Constr. Steel Res.* 36 (2) (1996) 101–119
5. P. Vila Real, J.-M. Franssen, Lateral Torsional Buckling of Steel - Beams in Case of Fire – Numerical Modelling. First International Workshop Structures in Fire, Copenhagen, 2000.
6. P. Vila Real, N. Lopes, L.S. da Silva, J.-M. Franssen, Lateral-torsional buckling of unrestrained steel beams under fire conditions: improvement of EC3 proposal, *Comput. Struct.* 82 (20) (2004) 1737–1744
7. P. Vila Real, R. Cazeli, L. S. da Silva, A. Santiago, e P. Piloto (2004), The effect of residual stresses in the lateral-torsional buckling of steel I-beams at elevated temperature. *J. Constr. Steel Res.*, Vol. 60, No. 3–5, pp. 783–793.
8. C. Couto, P. Vila Real, N. Lopes, B. Zhao (2016), Numerical investigation of the lateral-torsional buckling of beams with slender cross section for the case of fire. *Engineering Structures*, Vol. 106, pp. 410-421.
9. C. Couto, P. Vila Real, N. Lopes, B. Zhao (2016), Local buckling in laterally restrained steel beam-columns in case of fire. *J. Construct. Steel Res.*, Vol. 122, pp. 543-556.
10. C. Couto, E. Maia, P. Vila Real, N. Lopes (2018), The effect of non-uniform bending on the lateral stability of steel beams with slender cross-section at elevated temperatures. *Engineering Structures*, Vol. 163, pp. 153-156.
11. J.-M. Franssen, F. Morente, P. Vila Real, F. Wald, A. Sanzel, B. Zhao (2016). Fire Design of Steel Members with Welded or Hot-rolled Class 4 Cross-sections (FIDESC4).
12. N. Silvestre, P. B. Dinis, D. Camotim (2013). Developments on the Design of Cold-Formed Steel Angels. *J. Struct. Steel Res*, Vol 139, No. 5, pp. 680-694.
13. B. W. Schafer (2008). Review: The Direct Strength Method of cold-formed steel member design. *J. Construct. Steel Res*, Vol 64, pp. 766-778.
14. D. Popovic, G. J. Hancock, K. J. R. Rasmussen (2001). Compression tests on cold-formed angles loaded parallel with a leg. *J. Struct. Steel Res*, Vol 127, No. 6, pp. 600-607.
15. T. Ranawaka, M. Mahendran (2010). Numerical modelling of light gauge cold-formed steel compression members subjected to distortional buckling at elevated temperatures. *Thin-Walled Structures*, Vol 48, No. 4-5, pp. 334-344.
16. L. Laim, J. P. C. Rodrigues (2018). Fire design methodologies for cold-formed steel beams made with open and closed cross-sections. *Engineering Structures*, Vol. 171, pp. 759-778.
17. P. B. Dinis, D. Camotim, N. Silvestre (2010). On the local and global buckling behavior of angle, T-section and cruciform thin-walled members, *Thin-Walled Structures*, Vol 48, pp. 786-797.
18. R. Dabrowski (1988). On Torsional Stability of Cruciform Columns, *J. Constr. Steel Res.*, Vol. 9, pp. 51-59.
19. G. Chen, N. S. Trahir (2006). Inelastic torsional buckling strengths of cruciform columns, *Engineering Structures*, Vol. 16, No. 2, pp. 83-90.
20. N. S. Trahir (2012). Strength design of cruciform steel columns. *Engineering Structures*, Vol. 35, pp. 307-313.
21. A. Taras, R. Greiner (2007). Torsional and flexural torsional buckling – A study on laterally restrained I-sections, *J. Constr. Steel Res.* Vol. 64, pp. 725-731.
22. L. Possidente, N. Tondini, J.-M. Battini (2019). Co-rotational 3D beam element for torsional problems of steel structures in fire. *Proceedings of the 7th International Conference on Structural Engineering, Mechanics and Computation (SEMC 2019)*, September 2-4, 2019, Cape Town, South Africa.
23. L. Possidente, N. Tondini, J.-M. Battini (2018). Branch-switching procedure for post-buckling analyses of thin-walled steel members in fire. *Thin-Walled Structures*, Vol 136, pp. 90-98.
24. S. E. Quiel, M. E. M. Garlock (2010), Calculating the buckling strength of steel plates exposed to fire. *Thin-Walled Structures.*, Vol. 48, No. 9, pp. 684-695.
25. C. Couto, P. Vila Real, N. Lopes, B. Zhao (2015), Resistance of steel cross-sections with local buckling at elevated temperatures. *J. Construct. Steel Res.*, Vol. 109, pp. 101-114.
26. J. Jönsson, T.-C. Stan (2017), European column buckling curves and finite element modelling including high strength steels. *J. Construct. Steel Res.*, Vol 128, pp. 136-151  
Thomas, P. H., Webster, C. T. and Raftery, M. M., Experiments on Buoyant Diffusion Flames, *Combustion & Flame*, Vol. 5, 1961, pp. 359